



HAL
open science

Finite contact duration modeling of a Vibro-Impact Nonlinear Energy Sink to protect a civil engineering frame structure against seismic events

Stefania Lo Feudo, Stéphane Job, Miriam Cavallo, Aguinardo Fraddosio,
Mario Daniele Piccioni, Alessandro Tafuni

► To cite this version:

Stefania Lo Feudo, Stéphane Job, Miriam Cavallo, Aguinardo Fraddosio, Mario Daniele Piccioni, et al.. Finite contact duration modeling of a Vibro-Impact Nonlinear Energy Sink to protect a civil engineering frame structure against seismic events. 2020. hal-03039033v2

HAL Id: hal-03039033

<https://hal.science/hal-03039033v2>

Preprint submitted on 24 Mar 2022 (v2), last revised 24 Mar 2022 (v3)

HAL is a multi-disciplinary open access archive for the deposit and dissemination of scientific research documents, whether they are published or not. The documents may come from teaching and research institutions in France or abroad, or from public or private research centers.

L'archive ouverte pluridisciplinaire **HAL**, est destinée au dépôt et à la diffusion de documents scientifiques de niveau recherche, publiés ou non, émanant des établissements d'enseignement et de recherche français ou étrangers, des laboratoires publics ou privés.

Finite contact duration modeling of a Vibro-Impact Nonlinear Energy Sink to protect a civil engineering frame structure against seismic events

S. Lo Feudo^{a,*}, S. Job^a, M. Cavallo^{b,a}, A. Fraddosio^b, M.D. Piccioni^b, A. Tafuni^{b,a}

^aQUARTZ (EA 7393), VAST, Supméca – ISMEP, 3 Rue Fernand Hainaut, 93400 Saint-Ouen-sur-Seine, France

^bPolytechnic University of Bari, 4 Via Edoardo Orabona, 70126 Bari, Italy

Abstract

This paper proposes a finite contact duration model of a Vibro-Impact Nonlinear Energy Sink (VI NES) for controlling the vibrations of a civil engineering frame structure under seismic input. The device is composed of a container enclosing an inelastic sphere, interacting via a nonlinear viscoelastic dissipative force with the inner walls of the container. As the structure vibrates, the particle bounces within the container, exploring dynamical regimes ranging from periodic collisions to chaos and dissipating energy. Our VI NES is optimized for the El Centro NS (1940) earthquake signal, and its effectiveness in reducing the dynamic response of a ten-story frame structure is investigated. It is also compared with a classical TMD optimized according to the Den Hartog criterion. The main result is that the performance of the VI NES in reducing the top floor maximum displacement is very satisfying. Moreover, sensitivity analyses reveal good robustness of the VI NES to initial conditions and to variations in the properties of the primary structure.

Keywords: Vibro-impact damper, Nonlinear Energy Sink, contact mechanics, passive control, earthquake engineering

1. Introduction

Dynamic response of structures due to wind load and seismic excitation still remain a major concern in the field of civil engineering. The earliest device proposed for the passive control of vibrations is the Tuned Mass Damper (TMD), which is a linear mass-spring-dashpot oscillator added to a primary mass and tuned to one resonant frequency [1]. Several studies have been conducted in the past decades and a wide range of optimization criteria were proposed under various excitation regimes of the primary system [2–6].

Despite its well-known dynamic behavior, the major drawbacks of TMD are its sensitivity to the uncertainty of the primary structure, and its tunability with only one resonant frequency [7, 8]. Also, for high amplitude motions the primary structure can behave nonlinearly due to geometric nonlinearities, nonlinear external sources and damage, making TMD ineffective. Indeed, during its life-cycle a building can undergo several seismic events, which may affect the integrity of structural elements and change its overall dynamic properties. Even during one earthquake, if particularly severe, the structure might undergo damage capable of substantially changing its vibration features [9–11]. Moreover, the stiffening effect of filling walls is generally not considered in seismic design, and therefore in TMD optimization. Beside this, the brittle behavior of filling walls might lead to a sudden and significant decrease in stiffness during an earthquake [12–14].

For the seismic protection of buildings, several passive and active control strategies can be employed [15–19]. Also, in the last few years, many attempts have been made to develop new shapes and mechanical designs of nonlinear

*Corresponding author

Email addresses: stefania.lofeudo@supmeca.fr (S. Lo Feudo), stephane.job@supmeca.fr (S. Job), m.cavallo4@studenti.poliba.it, miriam.cavallo@edu.supmeca.fr (M. Cavallo), aginaldo.fraddosio@poliba.it (A. Fraddosio), mariodaniele.piccioni@poliba.it (M.D. Piccioni), a.tafuni2@studenti.poliba.it, alessandro.tafuni@edu.supmeca.fr (A. Tafuni)

vibration absorbers. Indeed, nonlinear devices can extend vibration control to a wide frequency range by ensuring high robustness and low sensitivity. For example, this is the case of tuned liquid dampers based on nonlinear sloshing [20, 21], friction dampers [22, 23] and hysteretic dampers [24].

Another promising technology is Nonlinear Energy Sinks (NES), which are essential nonlinear oscillators, i.e. oscillators without linear restoring force. Since an NES has no inherent eigenfrequency, it can in principle tune to any resonant frequency of the primary structure, by giving rise to an irreversible energy transfer from the main system to the NES above a certain excitation threshold, [25–28]. Previous studies have shown that this threshold increases with frequency, since NES requires the reception of very high input energy to start vibrating and activating the Targeted Energy Transfer (TET). This drawback reduces the effectiveness of NES in a Multi-Degrees Of Freedom (MDOF) system [29, 30]. From the technological point of view, an NES can be obtained, for example, by a mass moving transversely to elastic elements [31–33] and magnetic forces [30, 34, 35]. In the latter, negative stiffnesses lead to bistability. Subsequently, quasi-periodic or chaotic oscillations occur, improving the vibration absorption effect and reducing the minimal energy threshold for activating the TET [29, 36].

The present paper deals with the Vibro-Impact Nonlinear Energy Sink (VI NES) damper, according to the experimental set-up studied by [37–39]. The device is composed of a hollow rigid container hosting a deformable spherical particle. When the rigid box connected to the primary structure oscillates, the inner particle bounces and impacts against the edges, thereby dissipating energy. According to the general definition of the NES, the vibro-impact damper lacks linear stiffness and can damp the vibrations of a primary system over a wide frequency bandwidth. Moreover, due to its non-smooth dynamical behavior, the VI NES might undergo chaotic vibrations, potentially mitigating the force threshold for the TET. In [40] one and multiple VI NESs were added to a two degrees of freedom primary system under seismic excitation. The authors underlined that the VI NES has two beneficial effects on seismic mitigation. Firstly, TET takes place at the initial stage of the ground motion, when the primary structure is highly stressed. Secondly, VI NES redistributes energy to higher frequencies. The clearance of the VI NES, that is to say the difference between the size of the container and the size of the inner particle, has been identified as the design parameter that impacts most on maximum displacement reduction; its optimum value depends on the earthquake’s characteristics. The results were confirmed for a primary structure with more degrees of freedom in [41, 42]. Reference [43] suggested adopting multiple VI NESs in conjunction with NESs having cubic nonlinearity for seismic mitigation. Another relevant design parameter of the VI NES, the particle-to-container mass ratio, is generally constrained by technological requirements and by the absorber’s position over the primary structure, whereas the coefficient of restitution depends on the material properties and can be optimized under free vibrations [44].

The dynamics of the VI NES was studied experimentally and analytically in [37], wherein various vibrational regimes were observed. These regimes and their influence on the TET were accurately identified in [39, 45, 46]. Chaotic behavior was further analyzed through the analysis of the Lyapunov exponent in [39]. Energy dissipation due to impacts between multiple particles was investigated in [47, 48], while the technology and applications have been reviewed in [49, 50]. Recently, a single contact vibro-impact damper has been coupled to the Acoustic Black Hole effect for the passive vibration control of thin-walled structures [51, 52].

To the authors’ knowledge, in previous research on VI NES, the contact dynamics was generally treated as an instantaneous phenomenon including a phenomenological coefficient of restitution (COR). In [51, 52], the contact dynamics was considered as an non-instantaneous but purely conservative phenomenon. On the contrary, in the present study the particle is an inelastic sphere interacting with the inner walls according to the elasto-frictional Hertz Mindlin potential, [53], including more realistic nonlinear viscoelastic dissipative contributions [54–56]. This allows substantially improving the accuracy of the description of VI NES dynamics, and thus of its vibration absorption capability. In particular, in this paper the VI NES with a finite contact duration model is applied to the seismic control of a ten-story frame building. VI NES clearance is optimized, and the effectiveness of the VI NES is compared to that of the well-known TMD tuned to the first mode of the structure according to Den Hartog’s criterion [1]. The sensitivity of VI NES control performance to initial conditions and primary structure stiffness properties is also analyzed.

The paper is organized as follows. The VI NES is presented in Section 2. Several contact models, from the instantaneous model to the finite elastic *Hertz* and the viscoelastic models *Tsuji* and *Kuwabara*, are introduced to describe the interaction between the VI NES particle and the case walls. It is shown that the accuracy of modeling VI NES dynamics is enhanced by considering collisions with finite durations. The equations of motion of an MDOF system coupled with a VI NES are then presented. In Section 3 the properties of the case study, consisting of a civil engineering benchmark frame building are presented. A design criterion for the VI NES is introduced; the influence

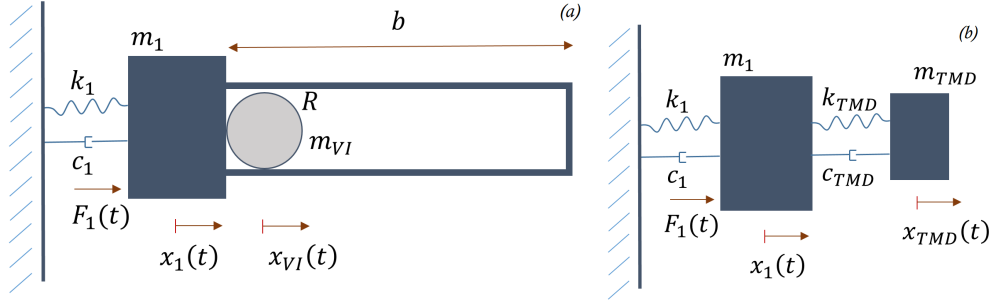


Figure 1: Schematic representation of (a) a VI NES and (b) a TMD.

of the initial conditions on the performance of the device is then analyzed. Furthermore, the seismic response of the overall system will be shown and discussed, also in comparison with the classical TMD. Then, a sensitivity analysis on the robustness of the device against the variation of stiffness, reproducing the possible damage of the primary structure, is carried out. Finally, the conclusions reached are provided in Section 4.

2. Vibro-Impact Nonlinear Energy Sink

The VI NES studied here is a development of the device considered in [37–39], and its schematic representation is shown in Figure 1(a). Generally speaking, the VI NES is composed of a spherical particle enclosed within a hollow mass-spring-dashpot system. When the box oscillates, the sphere moves by rebounding against the opposing edges. In the configuration considered here, the coupled system vibrates along the x axis, which is perpendicular to the direction of gravity. When vibrated vertically, the particle bounces inside the container and takes-off when the acceleration of the container exceeds gravity [48]. As in the previous research studies mentioned above, we made the choice to neglect the gravity effect and the friction between the particle and the bottom surface. Consequently, no rolling occurs and the VI NES has only one translational degree of freedom. In turn, we take into account the contact force and duration by implementing a viscoelastic dissipative contact model [54]. There are two reasons for this. Firstly, it has been proven that Targeted Energy Transfer (TET) strongly depends on the VI NES response regime, ranging from chaos to 1:1 resonance with two impacts per cycle [57, 58]. The latter is considered as the optimal condition for energy dissipation under harmonic excitation [38, 59]. As a consequence, a proper estimation of contact duration is needed in order to account for such a delay on the overall dynamics in the time domain, especially under random excitation [60]. Secondly, in the present case study collisions occur between a particle composing the VI NES and an MDOF oscillator. The so-called impulse–momentum model relying on COR (see below) is based on instantaneous impacts between perfectly rigid masses without any other external forces, so that momentum is exchanged between the colliding bodies only; this excludes any transfer of energy and momentum to underlying coupled oscillators. For instance, the presence of an elastic restoring spring beneath an impacted body modifies the energy balance and generates an inaccuracy in the estimation of the energy loss, since this secondary system is not taken into account in the model mentioned previously.

In Section 2.1, the theoretical models for elastic and viscoelastic contact are presented for the case of a ball bouncing on a fixed plate. Particular attention will be paid to the effect of finite contact duration on the system’s dynamics and on the estimation of the energy transfer in a coupled system. In Section 2.2 the equations of motions of an MDOF system endowed with a VI NES will be stated. In Section 2.3 the basic principles of TMD design and parameter optimization are recalled.

2.1. Contact models

In contact mechanics, collisions between bodies can be regarded in the framework of the kinematics of either rigid or deformable bodies. In the case of rigid bodies, an instantaneous contact generates a change in direction of a particle free to move, with possibly some energy loss and velocity variation. In the case of deformable bodies, linear, nonlinear elastic, viscoelastic or plastic deformations may occur during contact. Accordingly, a contact force law has

to be defined. Exhaustive literature reviews including pure elastic and dissipative contact force models were reported in [61, 62]. Taking into account the finite duration of the interaction and viscoelastic dissipation from a physical standpoint is a useful improvement with respect to previous research studies on VI NES. In the next subsections, the theoretical formulation of instantaneous and viscoelastic contact dynamics are detailed for the bouncing ball scheme. First, the basic principle governing instantaneous collisions between particles will be recalled. Then, nonlinear elastic (*Hertz*) and viscoelastic (*Tsuji, Kuwabara*) models are presented [54–56]. The range of validity and accuracy of instantaneous and finite collisions are discussed.

2.1.1. Instantaneous collision

The normal collision between two particles, with mass $m_{1,2}$ and velocity $v_{1,2}(t)$, generates a repulsive force which conserves linear momentum even within a non-conservative interaction, $m_{1,2}\partial_t v_{1,2}(t) = \pm F(t)$, leading to

$$m_1 v_1(t_c) + m_2 v_2(t_c) = m_1 v_1(0) + m_2 v_2(0), \quad (1)$$

where $t = 0$ is the initial collision time and t_c stands for the finite contact duration. Nevertheless, it is worth noting that the instantaneous collision case is obtained as a limit case for $t_c \approx 0$. According to Newton's law of restitution [63], the relative velocity after impact is proportional and opposite in direction to the relative velocity before impact, resulting in:

$$\epsilon = \frac{v_1(t_c) - v_2(t_c)}{v_2(0) - v_1(0)}, \quad (2)$$

where $0 \leq \epsilon \leq 1$ is called the coefficient of restitution. If the contact force is non-conservative, ϵ provides a measure of how much energy is dissipated during a binary collision, since it is possible to write:

$$K_r(t_c)/K_r(0) = \epsilon^2, \quad \text{where } K_r = \sum_{n=1}^2 (1/2)m_n(v_n - v_{CM})^2 \quad \text{and} \quad v_{CM} = \sum_{n=1}^2 m_n v_n, \quad (3)$$

K_r and v_{CM} are the relative kinetic energy and the velocity of the center of mass of the two particles, respectively. Now, by substituting Eq. 1 into Eq. 2 it is possible to determine the post-impact velocities.

$$v_{1,2}(t_c) = \frac{(m_1 \mp \epsilon m_{2,1})v_1(0) + (m_2 \pm \epsilon m_{2,1})v_2(0)}{m_1 + m_2}. \quad (4)$$

The value of the coefficient of restitution ranges from $\epsilon = 0$ for perfectly inelastic collision to $\epsilon = 1$ for perfectly elastic collision [53]. It can be determined experimentally by dropping a particle from an initial height above an elastic surface and by measuring the rebound velocity [64]. The advantage of this scalar parameter is that it can be easily handled but its precise value is not well referenced within standard databases of materials, first, because it stands for a rough approximation of complex physics, and second, because it is not an intrinsic feature of a material but results from the interaction between the two or more solids in contact.

The coefficient of restitution can also be determined from the measurement of the contact duration and the flight time of the particle between each bounce [65]. Generally, the contact duration t_c is very small when impacts occur between rigid bodies and is thus neglected, as an instantaneous collision approximation. In this regard, Ref. [60] experimentally validated an instantaneous collision model for a Single-Degree Of Freedom (SDOF) oscillator equipped with a vibro-impact damper composed by a steel particle and a fixed edge made of aluminum alloy. In the case study examined in [60], the contact time was found to be equal on average to 0.3 ms, which was considered sufficiently fast with respect to the natural period of the primary structure (0.25 s) to be neglected. However, in the next Sec. 2.1.2, we show that accounting for a finite contact duration is essential to make an accurate estimation of the energy dissipated by multiple impacts, even for a very fast contact duration. In addition, such a description allows a more suitable physical description of the dissipative mechanisms via a relaxation process in the bulk material of the particles.

2.1.2. Finite duration collision

i. Hertz model

According to the Hertzian interaction potential [53], the contact force F is

$$F(t) = C[\delta(t)]_+^{3/2}, \quad (5)$$

where δ is the overlap penetration between solids and $[\dots]_+$ denotes the Heavyside function, which relies on the absence of tensile force when the solids are not in contact. The prefactor C depends on the material properties and on the local radius of curvature near the contact area of the two bodies,

$$C = (4/3)E\sqrt{R}, \quad (6)$$

and it is defined in terms of a reduced elastic modulus E and a reduced radius R , both defined as follows:

$$E = [(1 - \nu_1^2)/E_1 + (1 - \nu_2^2)/E_2]^{-1} \quad \text{and} \quad R = (R_1^{-1} + R_2^{-1})^{-1}, \quad (7)$$

where ν_1 and ν_2 and E_1 and E_2 are the Poisson's ratios and the Young's moduli of the two materials, respectively, and R_1 and R_2 are the local radii of curvature of the two bodies near the contact zone.

The contact duration t_c can be estimated by applying the principle of conservation of energy, considering that the incident kinetic energy of two colliding particles has to be converted first into the elastic deformation of the contact region, before bouncing back. At the maximal deformation, when the particles stop deforming, the initial kinetic energy $K = (1/2)mv^2$ is fully stored in potential energy $U = \int Fd\delta = (2/5)C\delta^{5/2}$, where v is the relative contact velocity and $m = (m_1^{-1} + m_2^{-1})^{-1}$ is the reduced mass. Equality leads to $\rho R^3 v^2 \propto ER^{1/2}(vt_c)^{5/2}$, by approximating the deformation rate as $v \propto \delta/t_c$ and considering ρ as the mass density of the materials composing the bodies. Hence, by introducing the elastic wave speed in the bulk material of the particle, $c_w \propto \sqrt{E/\rho} \gg v$, and by introducing the elastic wave time-of-flight inside the particle $t_w \propto R/c_w$, one obtains

$$t_c \propto t_w(c_w/v)^{1/5} \propto t_w(R/\delta)^{1/4}. \quad (8)$$

It follows that $t_c \gg t_w$ at equilibrium, since $\delta \ll R$, which confirms the validity of the quasi-static approximation of the Hertz potential [53]. Additionally, the scaling given in Eq. 8 demonstrates that the contact duration t_c can be safely neglected only if one also neglects the time t_w taken for an elastic deformation to propagate through an elastic body. The latter may result in inconsistencies, the elasticity being taken into account on the one hand but neglected on the other hand. Moreover, bearing in mind that the position and the velocity of interacting bodies can change very quickly, a small error on the collision or rebound time can lead to a noticeable bias on the exact relative velocities, and consequently on the transfers of energy and momentum, as demonstrated in Sec. 2.1.3.

In this study, we aim at using a VINES to control the vibrations of a primary system, so the dissipative features of the contact law used for modeling impacts are crucial. To this end, we present in the next subsection two viscoelastic models, namely the *Tsuji* and the *Kuwabara* models. The former is fully relevant to the instantaneous model since it depends on the coefficient of restitution, but suffers from certain limitations which will be highlighted next. The latter will be preferred in our study since it relies on a viscoelastic relaxation time that provides more reliable estimations of the dissipated energy in most situations (multibody collisions, collisions involving elastic systems).

ii. Tsuji model

Here, we enrich the VINES model by introducing the viscoelastic contact law proposed in [55]. The contact force between the two particles previously introduced is evaluated as the sum of an elastic Hertzian and a dissipative term proportional to the indentation rate $\partial_t \delta$

$$F(t) = C[\delta(t)]_+^{3/2} + D\sqrt{Cm}[\delta(t)]_+^{1/4}\partial_t \delta(t), \quad (9)$$

where m is the reduced mass, and the prefactor D depends only on ϵ according to [56],

$$D(\epsilon) = \frac{-\sqrt{5} \ln(\epsilon)}{\sqrt{\ln^2(\epsilon) + \pi^2}}. \quad (10)$$

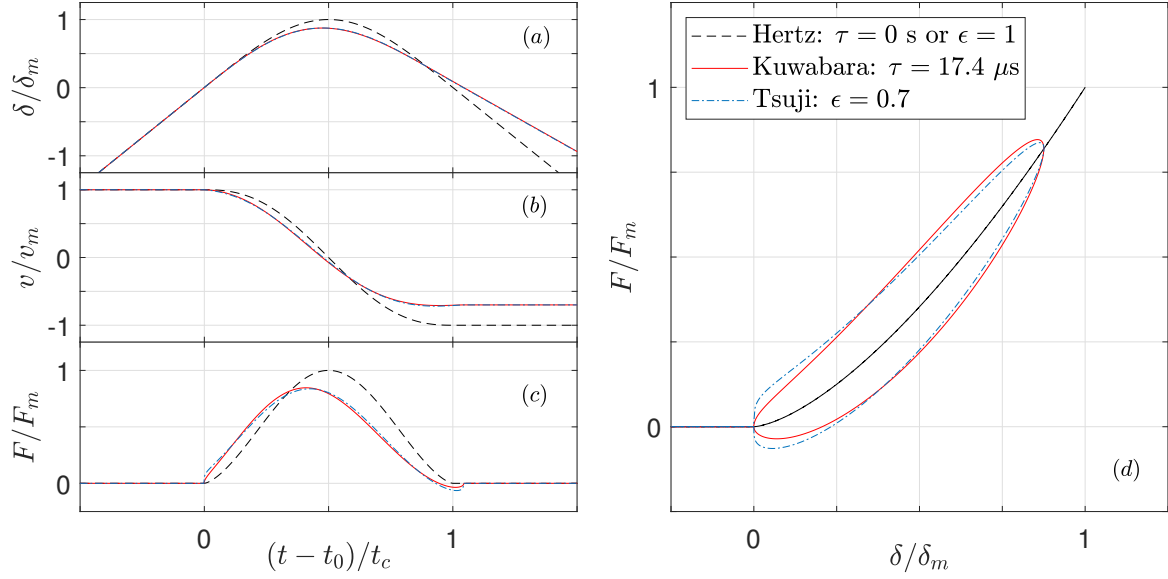


Figure 2: Contact between a steel particle of radius of 5 cm and a fixed plate. The initial velocity is $v_m = 1$ m/s. (a) Overlap deformation $\delta = (x - x_{plate})$, (b) deformation rate $v = \partial_t \delta$ and (c) repulsive force F of the contact as a function of time. (d) shows the force as a function of the deformation; the area within the curve is the dissipated energy. t_0 is the time of contact. The extrema δ_m and F_m and the contact duration t_c used to normalize all the curves refer to $\epsilon = 1.0$.

It is noteworthy that the instantaneous contact model given in Eq. 2 to 4, and the Tsuji model given in Eqs. 9 and 10, both fit for a collision between two masses only. These models neither fit for a collision between more than two bodies nor for a collision between a particle and a more complex elastic system (for instance a mass-spring element), as occurs for a VINES coupled to a frame structure. Indeed, in these cases part of the momentum and energy is leaked to external bodies, so that instantaneous contact and Tsuji model can provide unexpected/unpredicted energy dissipation values. To overcome this drawback, we introduce a model which accounts for a dissipation mechanism at the contact level only, namely the *Kuwabara* model.

iii. Kuwabara model

The description proposed by Kuwabara and Kono in [54] accounts for a viscous relaxation time τ relying on a Kelvin-Voigt material approximation. The relaxation results in a delay between the force and the deformation, hence $F(t) = C[\delta(t + \tau)]_+^{3/2}$. Assuming weak dissipation, $\omega\tau \ll 1$ where $\omega \propto 1/t_c$ stands for the typical frequency content of a collision, and using a first order Taylor expansion, one recovers the ansatz given in [54]:

$$F(t) \simeq C[\delta(t)]_+^{3/2} + (3/2)\tau[\delta(t)]_+^{1/2}\partial_t\delta(t). \quad (11)$$

The formulation given in Eq. 11 has been proven to be physically relevant [61, 64, 66]. It requires only the knowledge of the intrinsic relaxation time of the materials composing the solids in contact. This information is readily available for most materials, like for example steel, in terms of loss angle ϕ_{loss} or loss factor $\eta_{loss} = \tan(\phi_{loss}) = \omega\tau$, where $\omega \propto 1/t_c$ is given by Eq. 8.

Interestingly, it is possible to take advantage of the Tsuji model to relate τ and ϵ . Indeed, the comparison of Eq. 9 and Eq. 11 shows that the non-conservative term in Tsuji's approximation qualitatively results in a nonlinear relaxation time $\tau \propto \sqrt{m/C}(D/\delta^{1/4}) \propto (DR/c_w)(R/\delta)^{1/4}$, such that $\eta_{loss} = \omega\tau \propto D(\epsilon)$. This estimation tells that, in Tsuji's model, the ratio of the dissipated to the stored energy during a collision only depends on the coefficient of restitution, and consequently do not depend on either the strength or the rate of the resulting deformation. Hence, it is possible to estimate Kuwabara's relaxation time as $\tau \propto t_c(\delta) \times D(\epsilon)$, as seen below, from prior knowledge of a nominal indentation δ and a coefficient of restitution ϵ .

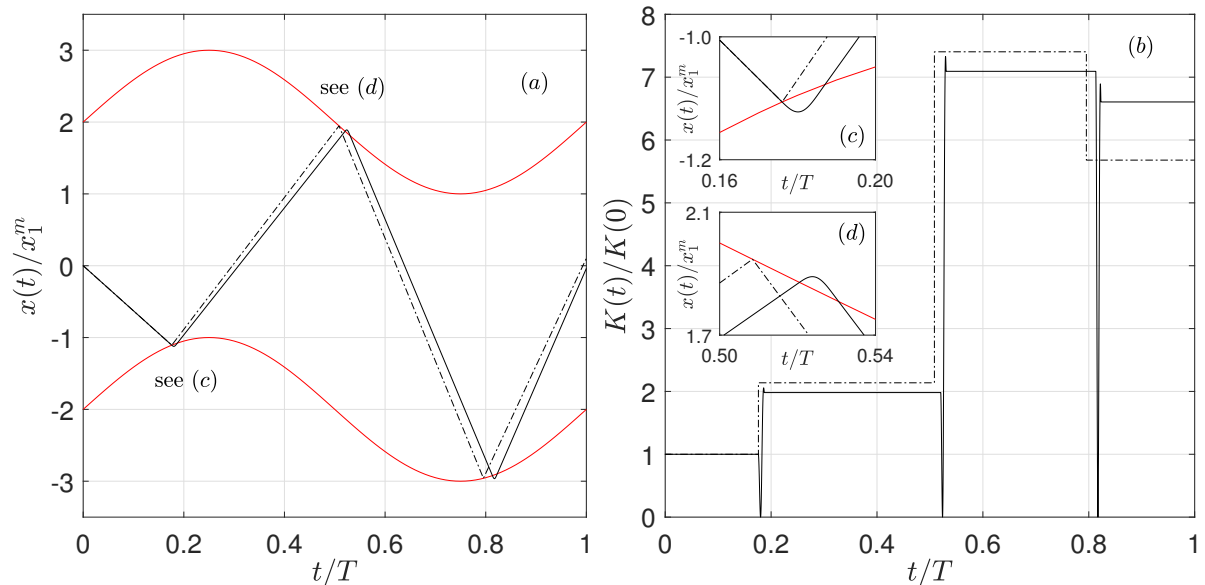


Figure 3: Simulated motion of the VI NES shown in Fig. 1(a). VI NES is a steel sphere of radius 5 cm, enclosed in a rigid cylinder of width $b = 40$ cm and diameter 10 cm, and shaken kinematically at $f = 1/T = 100$ Hz with an amplitude $x_1^m = 10$ cm (see the red solid curves). For the sake of clarity, the particle is considered as a point mass interacting with the inner walls of the container. (a) Position and (b) kinetic energy of the particle, according to instantaneous (black dashed line, see Eq. 4) and finite duration contact dynamics (black solid line, see Eqs. 9 and 10) for $\epsilon = 0.7$.

In order to demonstrate the equivalence of *Tsuji* and *Kuwabara* model, and their differences, we consider as an example in Fig. 2, a spherical particle of 5 cm radius thrown at an initial velocity of 1 m/s against an infinitely rigid and fixed wall. The particle is made of steel (mass density $\rho = 8000$ kg/m³, Young's modulus 210 GPa and Poisson's ratio 0.3) and the coefficient of restitution is set to an arbitrary value $\epsilon = 0.7$. In Fig. 2, these non-conservative models are compared to the conservative case of a Hertzian elastic model ($\epsilon = 1.0$). Here, both *Kuwabara* and *Tsuji* contact models rely on the same coefficient of restitution within $v_m = 1$ m/s, which requires setting a relaxation time $\tau = 17.4$ μ s for the former. Even within purely conservative mechanisms, the contact duration is finite due to the balance between inertia and elasticity. When viscoelasticity is taken into account, both the contact force and the maximal indentation become smaller and delayed between one and the other, see Fig. 2(a,c). The dissipated energy is represented by the area within the force-deformation loop, see Fig. 2(d). In Fig. 2(a,b) the particle displacement and velocity are shown. Owing to the similarity of the non-conservative mechanical responses, we choose to perform the case study presented in Sec. 3 using the *Kuwabara* model, which relies on a more physical, well documented, intrinsic dissipative mechanism.

2.1.3. Instantaneous versus finite duration collision

In this subsection, we provide examples, see Fig. 3, showing that a contact dynamics with finite duration has to be taken into account to obtain representative results even when the contact duration is small compared to the period of oscillation of a primary system, $t_c \ll T_1$. Such a requirement is even stronger when considering high eigenmodes (high frequency) of the primary system or soft/heavy particles (long contact duration). In addition, when considering the interaction between a particle damper and a resonant system, the finite duration ensures that a sudden change of direction at a rebound does not generate infinite deceleration and force, as in an instantaneous collision.

For the sake of side-by-side inspection, we here compare the instantaneous contact model given in Eq. 2 to 4 to *Tsuji's* finite duration contact model given in Eqs. 9 and 10, which both rely on the coefficient of restitution ϵ only. Here, no underlying mechanical system interacts with the colliding masses: the instantaneous model and *Tsuji's* model thus remain reliable and fully correspond to *Kuwabara's* model according to Sec. 2.1.2-iii. In Figure 3 we compare the two former. It can be seen that the first rebound introduces a delay between instantaneous and finite duration (*Tsuji*

model), which makes the second collision and the later ones, occur with different relative velocities. This leads to noticeably different estimations of the energy transfer from one to another, and thus of energy dissipation, even within a single period of oscillation, see insets (a) and (b). It is thus mandatory to resolve the contact dynamics, even if the contact duration appears negligible compared to the period of oscillation.

2.2. Equations of motion of MDOF system coupled with a VI NES

In this Section, the equations of motion of a system composed by an MDOF linear system enclosing a VI NES are presented. A schematic representation of the arrangement considered is depicted in Figure 1(a) in the case of an SDOF primary structure. First, let us consider the equations of motion of a linear MDOF system, representing a n -DOF primary structure or a $(n - 1)$ -DOF primary structure with a TMD representing the n -th DOF.

$$[\mathbf{M}] \partial_{tt} \{\mathbf{x}\} + [\mathbf{C}] \partial_t \{\mathbf{x}\} + [\mathbf{K}] \{\mathbf{x}\} = \{\mathbf{F}\}, \quad (12)$$

where $\{\mathbf{x}\} = \{x_1(t), x_2(t), \dots, x_n(t)\}^T$ is the displacement vector. In the case of n mass-spring-dashpot oscillators arranged in series, the mass $[\mathbf{M}]$, the damping $[\mathbf{C}]$ and the stiffness $[\mathbf{K}]$ matrices in Eq. 12 are given by:

$$[\mathbf{M}] = \begin{bmatrix} m_1 & 0 & \cdots & 0 \\ 0 & m_2 & & \\ \vdots & & \ddots & \\ 0 & \cdots & 0 & m_n \end{bmatrix}, \quad [\mathbf{C}] = \begin{bmatrix} c_1 + c_2 & -c_2 & 0 & \cdots & 0 \\ -c_2 & c_2 + c_3 & -c_3 & 0 & \vdots \\ 0 & -c_3 & \ddots & & 0 \\ \vdots & 0 & & c_{n-1} + c_n & -c_n \\ 0 & \cdots & 0 & -c_n & c_n \end{bmatrix}, \quad (13)$$

$$[\mathbf{K}] = \begin{bmatrix} k_1 + k_2 & -k_2 & 0 & \cdots & 0 \\ -k_2 & k_2 + k_3 & -k_3 & 0 & \vdots \\ 0 & -k_3 & \ddots & & 0 \\ \vdots & 0 & & k_{n-1} + k_n & -k_n \\ 0 & \cdots & 0 & -k_n & k_n \end{bmatrix}$$

where m_i , c_i and k_i are the mass, the damping coefficient and the stiffness of the i -th oscillator for $i = 1, \dots, n$.

The forces $\{\mathbf{F}\} = \{F_1(t), F_2(t), \dots, F_n(t)\}^T$ acting on the MDOF system as it is defined in Eq. 12, depend on whether the reference frame is Galilean or not. If the reference is Galilean, the former forces are ordinary external actions, and $\{\mathbf{x}\}$ represents the absolute displacements of the structure. On the contrary, in the case of seismic dynamics, one can consider Eq. 12 in the non-inertial reference frame of the oscillating ground, without external actions. In this situation, the resulting forces in Eq. 12 correspond to inertia forces, $F_i(t) = -m_i \gamma_G(t)$, where $\gamma_G(t) = \partial_{tt} x_G(t)$ stands for the absolute acceleration of the ground. In this case, $\{\mathbf{x}\}$ represents the motion of the structure relative to the moving reference [67].

Furthermore, when a VI NES is attached to the n -th oscillator, the equations of motion become:

$$[\mathbf{M}_{VI}] \partial_{tt} \{\mathbf{x}_{VI}\} + [\mathbf{C}_{VI}] \partial_t \{\mathbf{x}_{VI}\} + [\mathbf{K}_{VI}] \{\mathbf{x}_{VI}\} = \{\mathbf{F}_{VI}\}, \quad (14)$$

where

$$[\mathbf{M}_{VI}] = \begin{bmatrix} \mathbf{M} & \mathbf{0} \\ \mathbf{0} & m_{VI} \end{bmatrix}, \quad [\mathbf{C}_{VI}] = \begin{bmatrix} \mathbf{C} & \mathbf{0} \\ \mathbf{0} & 0 \end{bmatrix}, \quad [\mathbf{K}_{VI}] = \begin{bmatrix} \mathbf{K} & \mathbf{0} \\ \mathbf{0} & 0 \end{bmatrix}, \quad (15)$$

$\{\mathbf{x}_{VI}\} = \{\mathbf{x}(t), x_{VI}(t)\}^T$ and $\{\mathbf{F}_{VI}\} = \{\mathbf{F}, 0\}^T + \{\mathbf{0}, F_c, -F_c\}^T$ (where $\mathbf{0}$ is a vector of size $n - 1$).

It is noteworthy that $\{\mathbf{F}_{VI}\}$ is a nonlinear vector which depends explicitly on time, via the forcing $\{\mathbf{F}(t)\}$, and on the position and velocity of the Degree Of Freedom (DOF) via the contact force $F_c(x_{VI}, x_n, \partial_t x_{VI}, \partial_t x_n)$ acting between the VI NES and the upper DOF on which it stands, see for instance Eq. 9 or Eq. 11. In particular, F_c has no tensile contribution if the solids do not touch, so that $F_c[x_n(t) < x_{VI}(t) + R] = F[x_{VI}(t) > x_n(t) - R + b] = 0$. Otherwise, a

compressive force occurs when the bodies come into contact, inducing loss through elastic repulsion between them, according to Eq. 9 or Eq. 11.

The system of Eqs. 14 can be made non-dimensional by normalizing the forces by the magnitude $F_1 = m_1 \max \{|\gamma_G(t)|\}$ the displacements by $x_1 = F_1/k_1$ and the time by the natural frequency of the undamped lowest DOF of the primary system, $\omega_1 = \sqrt{k_1/m_1}$. By introducing the dimensionless displacement $X_i = x_i/x_1$ and the dimensionless time $\theta = \omega_1 t$, Eq. 14 becomes:

$$\partial_{\theta\theta} \{\mathbf{X}_{VI}\} + [\zeta_{VI}] \partial_{\theta} \{\mathbf{X}_{VI}\} + [\kappa_{VI}] \{\mathbf{X}_{VI}\} = \{\gamma_{VI}\}, \quad (16)$$

where $[\zeta_{VI}] = [\mathbf{M}_{VI}]^{-1} [\mathbf{C}_{VI}]/\omega_1$, $[\kappa_{VI}] = [\mathbf{M}_{VI}]^{-1} [\mathbf{K}_{VI}]/\omega_1^2$ and $\{\gamma_{VI}\} = (m_1/F_1) * [\mathbf{M}_{VI}]^{-1} \{\mathbf{F}_{VI}\}$. By also introducing the non-dimensional velocity $\{\mathbf{V}_{VI}\} = \partial_{\theta} \{\mathbf{X}_{VI}\}$, the dynamical system can be written in a state space form.

$$\frac{\partial}{\partial \theta} \begin{Bmatrix} \mathbf{X}_{VI}(\theta) \\ \mathbf{V}_{VI}(\theta) \end{Bmatrix} = \begin{bmatrix} \mathbf{0} & \mathbf{I} \\ -\kappa_{VI} & -\zeta_{VI} \end{bmatrix} \begin{Bmatrix} \mathbf{X}_{VI}(\theta) \\ \mathbf{V}_{VI}(\theta) \end{Bmatrix} + \begin{Bmatrix} \mathbf{0} \\ \gamma_{VI}(\mathbf{X}_{VI}, \mathbf{V}_{VI}, \theta) \end{Bmatrix}. \quad (17)$$

The latter system of differential equations gives rise to a stiff problem since two different time scales are involved in the system dynamics, one depending on the main system eigenvalues ω_i , and the other, faster, on the contact duration. To show this, let us consider the typical ratio of the eigenvalues $(\omega_i/\omega_{VI}) \simeq (k_i/m_i)^{1/2}/(k_{VI}/m_{VI})^{1/2} \propto (k_i/k_{VI})^{1/2} \epsilon_m^{1/2}$ with $\epsilon_m = m_{VI}/m_i \ll 1$. From Eqs. 5 - 6 one obtains the contact stiffness $k_{VI} = \partial F/\partial \delta \propto C\delta^{1/2} \propto ER(\delta/R)^{1/2}$. In the case of a primary structure represented by a multi-story building with square cross-sectional beams of width w_i and height L_i , stiffness coefficient is $k_i \propto Ew_i^4/L_i^3 \propto ER\epsilon_L^3$ with $w_i \sim R$, and $\epsilon_L = w_i/L_i \ll 1$. It turns out that according to Eq. 8, $(\omega_i/\omega_{VI}) \propto \epsilon_L^{3/2} \epsilon_m^{1/2} (R/\delta)^{1/4} \propto \epsilon_L^{3/2} \epsilon_m^{1/2} (c_w/v_{rms})^{1/5}$ with v_{rms} the typical amplitude of the seismic vibration velocity. For example, in the case of a primary structure under the seismic excitation *El Centro NS (1940)* reported in Sec. 3, for which the RMS velocity magnitude is $v_{rms} \simeq 6.7$ mm/s, a VI NES made of steel ($c_w \simeq 5500$ m/s) with $\epsilon_m = \epsilon_L = 10^{-1}$, we find the typical frequencies differ by at least one order of magnitude, $(\omega_i/\omega_{VI}) \sim 10^{-1}$. To handle the stiffness problem described in Eq. 17, we have chosen to perform the numerical integration by using MATLAB function ode45. This solver was preferred to ode23s, a lower order but stiff solver, owing to better accuracy, but at the cost of slower and heavier calculations.

2.3. Tuned Mass Damper

The Tuned Mass Damper is a linear device composed by an auxiliary mass-spring-dashpot linked to a primary structure and tuned with a resonant frequency, Fig. 1(b). In the case of dynamic loading near this frequency, the TMD starts to oscillate and dissipate a large amount of vibrational energy [1]. Generally, the TMD mass is fixed by technological requirements, and the stiffness and damping of the TMD are chosen according to proper optimisation criteria. The major criteria are based on the minimization either of the transfer function maximum or of the energy [68, 69], and on the pole location [70, 71]. The purpose of the Den Hartog criterion is to minimize the maximum amplitude of the primary system by properly setting the TMD's stiffness and damping. It is well known that in the case of an SDOF undamped primary structure, increasing the damping of the added mass to some extent reduces the amplitude at resonant frequency. For high damping coefficient, the two masses are virtually fused to each other and the amplitude at resonant frequency becomes infinite again. The first step of Den Hartog's criterion is to choose a frequency ratio $\lambda_{opt} = \omega_{TMD}/\omega_1$ for which the two resonant peaks have the same amplitude, and only then to search for the optimal damping ratio ξ_{opt} which minimizes the peak value. The approximate analytic solution of Den Hartog's criterion is given by [1]:

$$\lambda_{opt} = \frac{1}{1 + \mu_{TMD}} \quad \text{and} \quad \xi_{opt} = \sqrt{\frac{3\mu_{TMD}}{8(1 + \mu_{TMD})}}, \quad (18)$$

where $\mu_{TMD} = m_{TMD}/m_1$. This criterion can be extended numerically or algebraically for optimizing the TMD applied to damped and/or MDOF primary structures [72]. In the present paper, the performance of the TMD and of the VI NES will be compared in the case of controlling the vibration of an MDOF system. Here, the TMD is designed according to the optimal Den Hartog parameters.

Story	1	2	3	4	5	6	7	8	9	10
Mass (t)	179	170	161	152	143	134	125	116	107	98
Inter-story stiffness (MN/m)	62.47	52.26	56.14	53.02	49.91	46.79	43.67	40.55	37.43	34.31
Normalized first mode shape	0.175	0.355	0.534	0.708	0.871	1.019	1.146	1.248	1.321	1.359

Table 1: Mass, stiffness and normalized first mode of the ten-story shear-type frame examined.

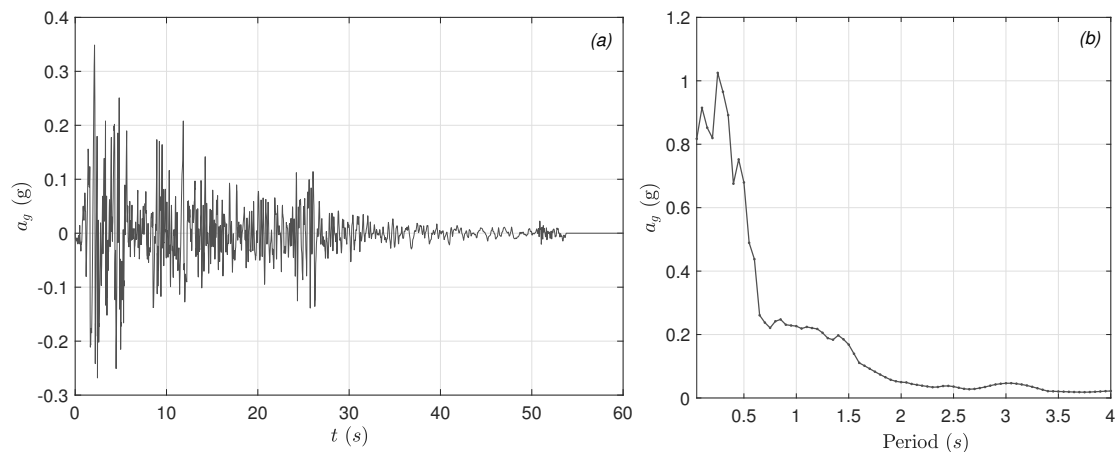


Figure 4: El Centro NS (1940) earthquake: (a) time history and (b) elastic response spectrum (damping ratio 2 %).

3. Passive control of a multi-story structure

3.1. The MDOF case-study and seismic excitation considered

To assess the effectiveness and the advantages of the VI NES as a seismic protection device for civil structures, numerical experiments were performed on a benchmark building. The choice of a benchmark case-study allows comparison with other control strategies. In particular, we consider the ten-story shear-type frame structure first proposed in [4] for numerical experiments on the structural control capability of TMDs against seismic excitations, and then examined for the same purpose in other studies, e.g., [2, 73].

The mass and inter-story stiffness properties of the structure considered are reported in Table 1. In order to compare them with the results in [4], according to [2] the damping matrix \mathbf{C} is assumed to be proportional to the stiffness matrix \mathbf{K} , with $\mathbf{C}(kNs/m) = 0.0129 \mathbf{K}(kN/m)$. Regarding the modal properties, the first mode of vibration (fundamental and lowest frequency mode) is characterized by a frequency of 0.5072 Hz and by a damping ratio of 2.06 %, with a participating mass over 80 %. The normalized mode shape of the first mode of vibration, relevant for determining the unit participation is also reported in Table 1.

To control possible earthquake-induced vibrations of the structure described above, we considered a suitably designed VI NES applied on the top of the 10-th floor; the strategy for the VI NES design is discussed in Section 3.2. The effectiveness of the VI NES in lowering seismic effects is also discussed in comparison with a classical TMD, again applied on the top of the 10-th floor. The latter was designed by assuming a mass ratio of 5 % of the modal mass of the first mode (see [3]), that is, $m_{TMD} = 55.97$ t, according to what is assumed in [2, 4, 73]. The TMD frequency and damping ratio were optimized by applying Den Hartog's criterion described in Section 2.3, obtaining $\lambda_{opt} = 0.9524$ and $\xi_{opt} = 0.1336$ respectively.

As the primary seismic excitation, we choose the well-known El Centro NS signal (1940), Figure 4. This seismic event is characterized by a relatively long effective ground motion duration, a relatively small value of Peak Ground Acceleration (PGA), and a quite narrow elastic response spectrum.

In Sec. 3.2, the VI NES clearance is optimized with reference to the earthquake introduced above in view of obtaining the most efficient seismic control of the ten-story shear-type frame examined in terms of response and

energy reduction. The effectiveness of the seismic protection of the VI NES is then discussed in Sec. 3.3 also in comparison with the optimized TMD. Finally, in Sec. 3.4 sensitivity analyses are proposed to discuss the variation in the seismic response induced by possible damage to the structure. It is worth noting that sensitivity analyses are crucial for assessing the effectiveness of a nonlinear damper like the VI NES; indeed, it is necessary to rule out undesired reductions of the seismic protection capacity due to parameter variations consistent with the expected uncertainties. Therefore, in Sec. 3.2 the sensitivity of the seismic control capacity of the VI NES regarding variations of the initial conditions in terms of initial displacements and/or initial velocity of the particle, is studied by a significant campaign of numerical experiments.

3.2. Optimal design of VI NES

In contrast to the case of TMD, there are very few studies in the literature on design criteria regarding the search for the optimal configuration of VI NES, especially with reference to seismic applications. Moreover, the problem is complicated because a nonlinear device like VI NES may show high sensitivity to parameter variations. Thus, a parametric study must be performed to identify the optimal values of the parameters governing VI NES dynamics. In order to suitably choose the objective function for such a parametric study, it is noteworthy that in the literature on the seismic protection of civil structures the effectiveness of a seismic device is generally expressed in terms the reducing the maximum absolute or inter-story displacements, or reducing the energy injected into the structure and directly connected to the stress level (elastic energy), or both parameters [74–77]. Here, we report the results of both the reduction of the maximum displacement of the top floor and of the cumulative elastic energy, that is the portion of the energy injected by the earthquake in the structure, absorbed by the structural members of the frame through elastic deformations. However, the first aspect generally prevails since during an earthquake the highest values of acceleration usually occur within a short time, after which a marked reduction of excitation takes place. Thus, a seismic control device has to be designed mainly to reduce vibration amplitude, and therefore the internal actions on the structural members, especially for the high-intensity part of the seismic event. More specifically, the reduction of the elastic energy gives a measure of the overall capability of the seismic device in controlling structural motions excited by the earthquake, whereas the maximum displacement of the top floor is more directly linked to the maximum level of the internal stresses. The latter is thus more essential for assessing if the structure will collapse or not during the seismic event considered, depending on its strength characteristics.

Regarding the optimization of VI NES, to give a clearer technical meaning to the comparison with TMD, we chose to fix one of the relevant parameters of VI NES, that is the particle mass, to be the same as the mass of the TMD ($m_{VI} = 55.97$ t). Moreover, we consider that the box and particle are made of steel (mass density $\rho = 8000$ kg/m³, Young’s modulus 210 GPa and Poisson’s ratio 0.3). Regarding the discussion in Sec. 2.1.2-iii, the energy loss during the contacts can be represented accurately by *Kuwabara’s* model. The relaxation time τ is set such that it results in a restitution coefficient $\epsilon = 0.7$ in the velocity range explored by the El Centro NS (1940) earthquake, see Fig. 2 and Fig. 4. The above assumptions considerably simplify the optimization of VI NES, since the only parameter to be determined is the clearance, represented by the dimensionless parameter $\beta = b/2R$, with b being the length of the box and R the radius of the sphere, the latter being considered assigned once fixed for the mass and the material (and hence the mass density).

In particular, the optimization of the VI NES was carried out by numerical simulations concerning the response of the ten-story shear-type frame considered under the action of the benchmark earthquake El Centro NS (1940). The objective functions to be minimized in the parametric study are represented by the displacement response reduction ratio x_r and the energy reduction ratio E_r given by

$$x_r = \frac{\max \{|x_{10}^{w/o}|\} - \max \{|x_{10}^w|\}}{\max \{|x_{10}^{w/o}|\}}, \quad E_r = \frac{E_e^{w/o} - E_e^w}{E_e^{w/o}}. \quad (19)$$

In Eq. 19, $x_{10}^{w/o}$ is the horizontal displacement relative to the ground of the top floor of the frame without control devices (uncontrolled structure), x_{10}^w is the horizontal displacement relative to the ground of the 10-th floor of the structure controlled by the VI NES, $x_{10}^w = x_{10}^{VI}$, or by the TMD, $x_{10}^w = x_{10}^{TMD}$; $E_e^{w/o}$ is the total elastic energy injected in the uncontrolled structure by the earthquake and E_e^w is the total elastic energy injected by the earthquake in the

structure controlled by the VI NES or the TMD, $E_e^w = E_e^{VI}$ or $E_e^w = E_e^{TMD}$. The maximum values are evaluated by referring to the whole duration of the accelerogram shown in Fig. 4.

Let us first consider the case of zero initial conditions, that is, the particle composing the VI NES is at rest and in contact with a wall of the box at the beginning of the seismic signal. The main results of the parametric study on β are summarized by Figure 5 (dashed line with unfilled markers), which shows that for El Centro NS (1940), the effectiveness of VI NES in reducing the response of the structures increases as β increases until the value $\beta = 1.35$ and then decreases. The same occurs for the energy reduction: the value of β that allows the maximum effectiveness of seismic control is again $\beta = 1.35$. It is worth noting that for all the parameters considered, moving away from the optimal value $\beta = 1.35$ significantly affects the seismic performance of the VI NES, especially concerning the maximum displacement reduction. Indeed, for too low or too high values of β it turns out that the device under investigation is incapable of controlling the first phase of the motion, where the largest displacements occur (see, also, Figure 6). On the other hand, in terms of overall elastic energy values, far from the optimal β the reduction of the VI NES's effectiveness is less marked. Moreover, in Figure 5 it can be clearly seen that for several ranges of β , the VI NES is distinctly more effective than the optimized TMD in reducing the maximum displacements (and thus the maximum internal forces), whereas the optimized TMD determines a more marked reduction of the elastic energy whatever the value considered for β .

Studying the sensitivity of seismic protection performances to the variation of the initial conditions (IC) in terms of initial displacements and/or initial velocity of the particle is a crucial aspect when optimizing VI NES parameters. Indeed, due to the high nonlinearity of VI NES, it is not possible to exclude in advance that the effectiveness of the device might be substantially lowered if an earthquake occurs when the particle is at rest but is neither in contact with box's walls, nor has zero velocity due to a forerunner earthquake motion (not zero IC). To assess the sensitivity of VI NES performances with the ICs, a systematic campaign of numerical experiments was performed. In particular, the ICs in terms of displacement are varied across 33 values within the range $[0, b]$ and the ICs in terms of velocity are varied across 33 values within the range $[-\max\{|v_{10}^{w/o}\}, \max\{|v_{10}^{w/o}\}|]$, where $\max\{|v_{10}^{w/o}\}|$ is the maximum velocity of the 10-th floor determined for the zero IC case without any control device. Therefore, overall, the seismic protection performances of the VI NES were studied for a set of more than one thousand different ICs. For the sake of comparison, a similar sensitivity analysis was performed when the structure was equipped with a TMD.

The results of the sensitivity analyses described above are summarized in Fig. 5 (solid line with filled markers), which also presents average values and standard variations, σ_{VI} and σ_{TMD} , of reduction ratios x_r and E_r obtained by varying the initial conditions. One can clearly see that the VI NES is weakly sensitive to the ICs and thus that the optimum β is quite robust. In particular, the analyses show that for $\beta = 1.35$, the maximum displacement reduction achieved by VI NES x_r ranges from 21.7 % to 30.3 %, over performing the optimized TMD ($11.7 \% \leq x_r \leq 23.7 \%$). On the other hand, in terms of elastic energy the TMD provides a better reduction ($71.7 \% \leq E_r \leq 80.7 \%$) than VI NES ($53.1 \% \leq E_r \leq 67.9 \%$). The results are reported in Table 2. Further analyses performed by the authors but not shown here for the sake of brevity, allow stating that the initial displacements of the particle have less influence on the seismic mitigation capacity of VI NES than the initial velocity. However, a scenario with high initial velocity is somewhat meaningless for a civil engineering structure since, in the case of earthquake, a building is first reached by primary waves having much lower amplitude than secondary waves.

In conclusion, we chose the value $\beta = 1.35$ for determining the length of the box of the optimized VI NES, since this value allows the best seismic response control with reference to the modal features of the structure considered and to the spectral features of the earthquake considered. Table 3 summarizes the main parameters characterizing the optimized VI NES.

Device	Reduction ratio	Reference case	Average	Standard deviation σ
VI NES	x_r	29.2 %	26.0 %	4.3 %
TMD	x_r	13.1 %	17.7 %	6.0 %
VI NES	E_r	67.2 %	60.5 %	7.4 %
TMD	E_r	77.5 %	76.2 %	4.5 %

Table 2: Performance sensitivity of VI NES ($\beta = 1.35$) and TMD to initial conditions. The reference case denotes results for the VI NES and TMD initially at rest. Average and Standard deviations are calculated from 33^2 different initial conditions.

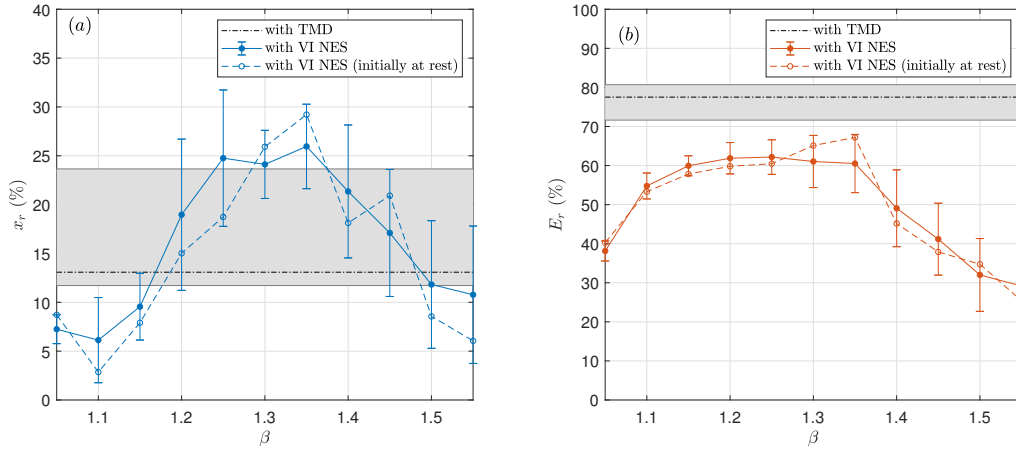


Figure 5: Parametric study on the effectiveness of the VI NES in controlling the structure under the El Centro NS (1940) earthquake. (a) Reduction of the maximum 10-th floor lateral displacement relative to the ground. (b) Reduction of the cumulative elastic energy. Average value and standard variations are calculated from 33^2 different IC. The line with unfilled markers stands for the VI NES initially at rest, the line with filled markers stands for average, vertical lines stand for $\pm\sigma_{VI}$. The horizontal dashed line stands for the TMD initially at rest, the gray shaded region stands for the interval mean $\pm\sigma_{TMD}$.

3.3. Seismic response results and discussion

Seismic behaviour of the ten-story shear-type frame considered under the El Centro NS (1940) earthquake is now discussed. The main features of the response are presented for the structure with and without the VI NES control device; moreover, the VI NES's response reduction capability is compared with that of a classical TMD. Both seismic devices have been optimized with respect to the structure examined and, for the VI NES, also to the earthquake considered, according to what is described in Sec. 3.1 and in Sec. 3.2. As for the initial conditions, VI NES is at rest and the particle is in contact with the rigid box's left-side. Figure 6 represents the time history of the lateral displacements of the 10-th floor for the uncontrolled structure, for the structure controlled by the VI NES, and for the structure controlled by the TMD. It is clear that the optimal definition of the VI NES parameters allows for a marked displacement mitigation especially during the first 15 sec of the earthquake, i.e. during the time when maximum displacements occur, and therefore when the most severe effects on the structure take place. In particular, the reduction of the maximum displacement is 29.2 %, whereas the optimized TMD is much less capable of controlling the structure in the first seconds of motions, with a reduction of the maximum displacement of 13.1 %. On the other hand, TMD allows for a more marked lowering of the response in the low-intensity part of the accelerogram.

In Figure 7, the time-history of the displacement of the two opposite walls of the box and of the particle of the VI NES are represented. It is evident that the high efficiency of VI NES in limiting the maximum displacements is linked to the fact that in the first instants, when the highest accelerations occur, the particle impacts both walls at each cycle of motion (two impacts in a period of oscillation). This generates head-on collisions that impede the motion and hence limit the amplitude of displacement. Afterwards, a diminution of the number of the impacts is observed, resulting in a decrease of the effectiveness in structural control.

The efficiency of VI NES can also be discussed in the light of the reduction of the cumulative elastic energy associated with the elastic deformations of the frame members. Since the latter are directly related to stresses in the frame elements, the relevance of this energy component in understanding the seismic behavior of the structure, and the importance of its reduction for seismic protection purposes are clear. Figure 8 shows the cumulative elastic energy

Material	ϵ	m_{VI} (t)	$2R$ (m)	b (m)
Steel	0.7	55.79	2.37	3.20

Table 3: Properties of the VI NES optimized for El Centro NS (1940) earthquake.

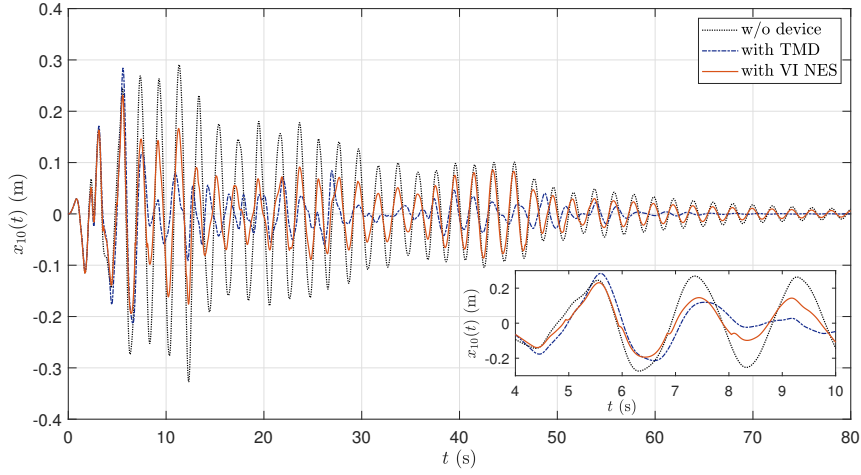


Figure 6: Time history of the lateral displacement of the 10-th floor. Comparison between the uncontrolled structure (w/o device) and the structure controlled by the VI NES and the TMD.

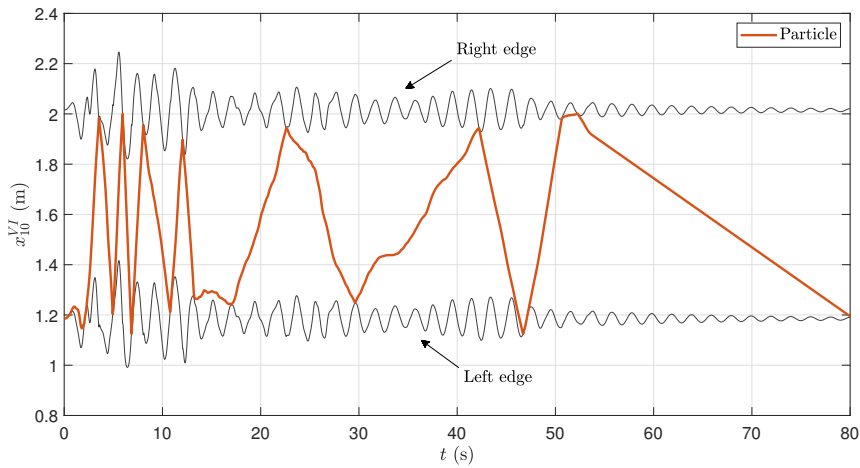


Figure 7: Time history of the displacement of the opposite walls and of the particle of VI NES.

for the uncontrolled structure, for the structure controlled by VI NES, and for the structure controlled by TMD. It can be readily seen that in the first 10 seconds of motion, when the seismic *main bang* occurs, the VI NES yields the highest energy reduction, whereas TMD is characterized by the best overall performances with respect to the whole duration of the accelerogram. However, it is interesting to observe that both seismic protection devices allow for a marked reduction in the energy associated with structural deformations.

Finally, Figure 9 provides a more in-depth description of the effects of VI NES in terms of controlling structure considered under earthquake excitation, representing the relative displacements of each floor of the structure, and the inter-story drifts relative to each story. Again, a comparison with TMD is made. The good performance of the VI NES stands out. Indeed, for the structure examined this device provides more efficient control of motion than the TMD.

In brief, the analyses performed show that VI NES can be effective as a seismic protection device, and that its effectiveness can be even higher than that of a classical TMD, at least if one considers the performance in terms of maximum relative displacement reduction, a crucial aspect for avoiding structural collapse. On the other hand, TMD shows better performance in the final part of the accelerogram, when the structural motion slows down.

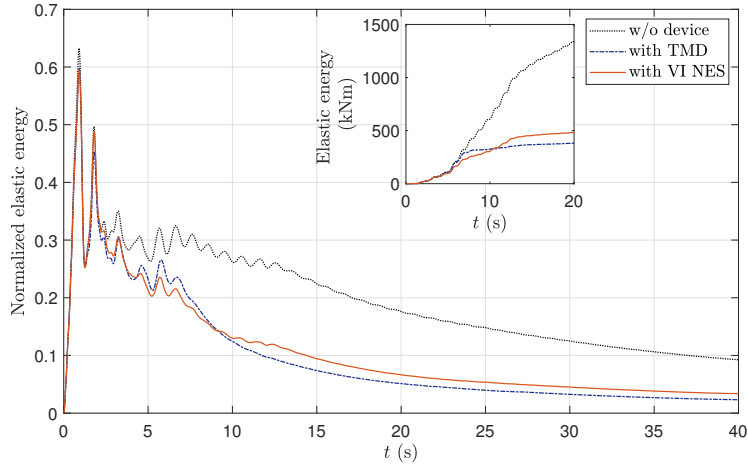


Figure 8: Cumulative elastic energy for the uncontrolled structure, for the structure controlled by the VI NES, and for the structure controlled by the TMD. Normalization is performed with respect to the injected energy.

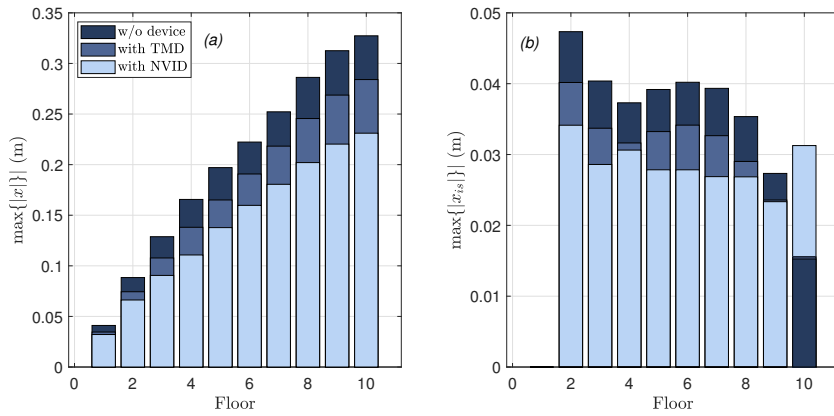


Figure 9: Seismic response at each floor of the frame structure controlled by the VI NES and the TMD. (a) maximum displacement, $\max\{|x|\}$, and (b) maximum inter-story drift, $\max\{|x_{i,i+1}|\}$.

3.4. Sensitivity analysis on the influence of the damage

To study seismic effects on a structure, the spectral features of the earthquake have to be coupled to the natural frequencies of the structure; this coupling is even more essential when seismic protection devices are employed. For example, by its nature the TMD has to be tuned with respect to one modal frequency of the structure to be controlled (typically, the first one), and a variation of this frequency might lead to an unexpected and significant decrease of the control capacity of the device. The same holds, in principle, for the VI NES, even if a broad band nonlinear vibration absorber is more robust with respect to changes in modal features or uncertainties of the primary structure. In the field of seismic engineering, one of the main sources of uncertainties is represented by stiffness. Indeed, the latter is difficult to determine since it is often difficult to accurately quantify the stiffness of secondary elements like partitions and external walls, and to accurately describe the interaction between primary structural elements and secondary elements of the construction. Moreover, seismic events could considerably damage secondary elements, and also primary structural elements might suffer from non-negligible damage. The latter results in a substantial variation of stiffness, and therefore in a marked alteration of natural frequencies that could lead to a decrease of the efficiency of structural control devices.

In order to study the robustness of the VI NES's performance with regard to variations of the structure's stiffness,

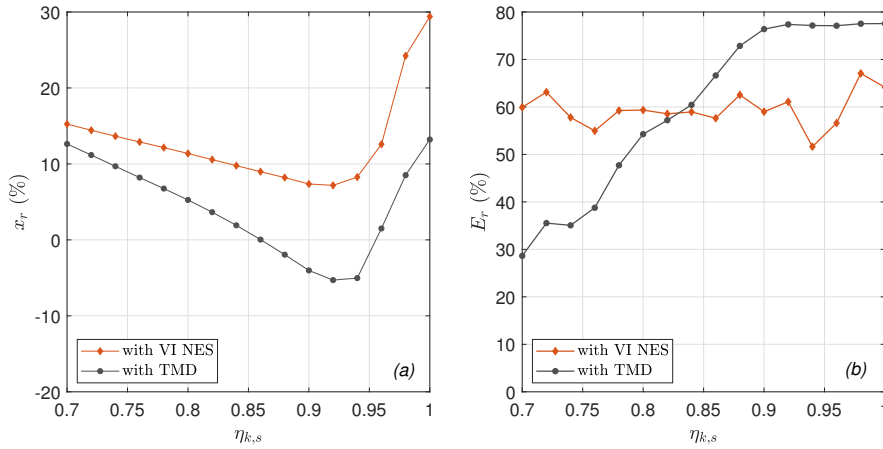


Figure 10: Sensitivity analysis on the variation of the stiffness of the primary structure. (a) Reduction of the maximum 10-th floor lateral displacement relative to the ground. (b) Reduction of the cumulative elastic energy.

a sensitivity analysis was carried out by varying the stiffness from 100 % to 70 % with respect to the nominal one, and keeping the other structural parameters fixed at the values described in Section 3.1 and the VI NES parameters at those presented in Table 3.

The results of this analysis are summarized in Figure 10, where the maximum relative displacement of the 10-th floor and the reduction of the cumulative elastic energy are represented versus the ratio $\eta_{k,s}$ between the stiffness considered in the calculation and the nominal stiffness of the structure (when $\eta_{k,s}$ is equal to 1, the primary structure is undamaged). As Figure 10 shows, the classical TMD suffers more than the VI NES from a loss of efficiency when the stiffness moves away from the design value. Whatever the case, the VI NES's performance is also lowered by the alteration of the stiffness, although the efficiency in terms of reductions of relative displacements is above 8 % for all the stiffness values considered. On the other hand, for the TMD a small variation of the stiffness ($\eta_{k,s} = 0.90 \div 0.95$) induces a sharp decay of the efficiency, and even renders the presence of the device counterproductive, with maximum displacements larger than those of the uncontrolled structure. From the point of view the reducing the cumulative elastic energy the capacity of the VI NES varies very little as $\eta_{k,s}$ varies, whereas the efficiency of the TMD falls significantly below $\eta_{k,s} = 0.90$. This makes the VI NES better from all points of views and very robust to the evolution of the primary system.

4. Conclusion

The analyses presented in this paper reveal that the VI NES provides promising results for the vibration control of a civil engineering frame structure under seismic excitation. As already pointed out in previous studies on VI NES, the clearance, which is related to the ratio of the box length and the particle diameter, appears to be a relevant design parameter. The optimal value in view of control efficiency is highly related to the ground motion acceleration and thus also to the soil characteristics. On the contrary, a sensitivity analysis on initial displacement and velocity of the particle highlights the good robustness of the VI NES against initial conditions, at least for the case study considered. The performances of the VI NES and TMD for the seismic mitigation of a ten-story building were compared in terms of maximum displacement at the top floor and cumulative elastic energy. The analyses performed revealed that higher vibration absorption is achieved by the VI NES at the beginning of the earthquake, where nearly a 1:1 resonance between primary structure and particle occurred. The maximum displacement of the top floor was reduced by about 30 %, exceeding the performance of the TMD, whereas for the reduction of the total elastic energy the TMD appeared to be more effective. In our opinion, the above results are noteworthy since the development of the VI NES for seismic applications is in its early stages, whereas the history of studies on the TMD for controlling earthquake induced dynamics covers many decades. A sensitivity analysis was conducted to evaluate the robustness of the vibration

absorber's performances in the case of variation of the primary structure modal properties, for example due to damage. In particular, when primary structure damage ranges from 0 to 30% in terms of stiffness, the performance of the TMD was degraded, whereas the effectiveness of the VI NES remained practically unchanged in terms of elastic energy reduction.

The VI NES is a non-smooth nonlinear system and its dynamics is greatly affected by the velocity of collision, contact duration and initial conditions. To ensure the accuracy of numerical simulations, a contact mechanics model with finite duration was considered, wherein the viscoelastic contact force was estimated according to the *Kuwabara* model.

In further developments, the VI NES model should be improved and validated with experimental measurements, by also taking into account the lateral friction and rotational motion of the particle. Moreover, a different design of the device is under investigation, aiming at obtaining a seismic device acting in all directions and under coupled motions, and thus capable of controlling 3D structures. It should be noted that this is only one of several possible technological evolutions of the VI NES concept, since many other research perspectives remain open, for example, the use of multi-particle devices, the use of one VI NES for each floor, the filling of the VI NES box with viscous or even magneto-rheological fluids (to achieve an active VI NES), studying the damage of the box walls and/or the fracture of the particle for maximizing dissipation in the case of exceptional seismic events. Finally, an in-depth systematic analysis of random excitation signals using appropriate statistical techniques should be performed to determine the robustness of the optimization of the VI NES subjected to different seismic signals.

CRediT

Stefania Lo Feudo: Conceptualization, Investigation, Methodology, Numerical simulations, Project administration, Writing. **Stéphane Job:** Conceptualization, Formal analysis, Investigation, Methodology, Numerical simulations, Writing. **Miriam Cavallo:** Investigation, Numerical simulations, Writing. **Aguinaldo Fraddosio:** Conceptualization, Investigation, Methodology, Writing. **Mario Daniele Piccioni:** Conceptualization, Investigation, Methodology, Writing. **Alessandro Tafuni:** Investigation, Numerical simulations, Writing.

Acknowledgment

This research was partially supported by Erasmus+ programme of the European Union through Master's students mobility. We thank Anne-Laure Vialette (ISAE-ENSMA) and Antoine Faulconnier (Supméca Groupe ISAE) for their contribution given at the early stages of this study (Software).

Founding

This research did not receive any specific grant from funding agencies in the public, commercial, or not-for-profit sectors.

References

- [1] J. Den Hartog, *Mechanical Vibrations*, McGraw - Hill, New-York, 1934.
- [2] M. Hadi, Y. Arfiadi, Optimum design of absorber for MDOF structures, *Journal of Structural Engineering* 124 (11) (1998) 1272 – 1280. doi:10.1061/(asce)0733-9445(1998)124:11(1272).
- [3] R. Rana, T. Soong, Parametric study and simplified design of tuned mass dampers, *Engineering Structures* 20 (3) (1998) 193–204. doi:10.1016/s0141-0296(97)00078-3.
- [4] F. Sadek, B. Mohraz, A. Taylor, R. Chung, A method of estimating the parameters of tuned mass dampers for seismic applications, *Earth Eng Struct Dyn* 26 (6) (1997) 617–635. doi:10.1002/(sici)1096-9845(199706)26:6<617::aid-eqe664>3.0.co;2-z.
- [5] C. Lee, Y. Chen, L. Chung, Y. Wang, Optimal design theories and applications of tuned mass dampers, *Engineering Structures* 28 (1) (2006) 43–53. doi:10.1016/j.engstruct.2005.06.023.
- [6] G. Bekdaş, S. Nigdeli, Estimating optimum parameters of tuned mass dampers using harmony search, *Engineering Structures* 33 (9) (2011) 2716–2723. doi:10.1016/j.engstruct.2011.05.024.
- [7] H. Yu, F. Gillot, M. Ichchou, Reliability based robust design optimization for tuned mass damper in passive vibration control of deterministic/uncertain structures, *Journal of Sound and Vibration* 332 (9) (2013) 2222–2238. doi:10.1016/j.jsv.2012.12.014.

- [8] S. Krenk, J. Hogsberg, Tuned mass absorber on a flexible structure, *Journal of Sound and Vibration* 333 (2014) 1577–1595. doi:10.1016/j.jsv.2013.11.029.
- [9] F. Légeron, P. Paultre, J. Mazars, Damage mechanics modeling of nonlinear seismic behavior of concrete structures, *Journal of Structural Engineering* 131 (6) (2005) 946–955. doi:10.1061/(asce)0733-9445(2005)131:6(946).
- [10] X. Ji, G. Fenves, K. Kajiwara, M. Nakashima, Seismic damage detection of a full-scale shaking table test structure, *Journal of Structural Engineering* 137 (1) (2011) 14–21. doi:10.1061/(asce)st.1943-541x.0000278.
- [11] C. Ramirez, A. Liel, J. Mitrani-Reiser, C. Haselton, A. Spear, J. Steiner, G. Deierlein, E. Miranda, Expected earthquake damage and repair costs in reinforced concrete frame buildings, *Earthquake Engineering and Structural Dynamics* 41 (11) (2012) 1455–1475. doi:10.1002/eqe.2216.
- [12] I. Koutromanos, A. Stavridis, P. Shing, K. William, Numerical modeling of masonry-infilled rc frames subjected to seismic loads, *Computers and Structures* 89 (11 - 12) (2011) 1026–1037. doi:10.1016/j.compstruc.2011.01.006.
- [13] A. Stavridis, I. Koutromanos, P. Shing, Shake-table tests of a three-story reinforced concrete frame with masonry infill walls, *Earthquake Engineering and Structural Dynamics* 41 (6) (2012) 1089 – 1108. doi:https://doi.org/10.1002/eqe.1174.
- [14] H. Zhang, J. Kuang, T. Yuen, Low-seismic damage strategies for infilled rc frames: shake-table tests, *Earthquake Engineering and Structural Dynamics* 46 (14) (2017) 2419 – 2438. doi:https://doi.org/10.1002/eqe.2911.
- [15] M. Symans, M. Constantinou, Semi-active control systems for seismic protection of structures: A state-of-the-art review, *Engineering Structures* 21 (6) (1999) 469–487. doi:10.1016/s0141-0296(97)00225-3.
- [16] T. Soong, B. Spencer, Supplemental energy dissipation: state-of-the-art and state-of-the-practice, *Engineering Structures* 24 (3) (2002) 243–259. doi:10.1016/s0141-0296(01)00092-x.
- [17] C. Christopoulos, A. Filiatrault, *Principle of Passive Supplemental Damping and Seismic Isolation*, IUSS Press, 2006.
- [18] I. Takewaki, *Building Control with Passive Dampers: Optimal Performance-based Design for Earthquakes*, Wiley, 2009.
- [19] Z. Liang, G. C. Lee, G. F. Dargush, J. Song, *Structural Damping Applications in Seismic Response Modification*, CRC Press, 2011.
- [20] A. Di Matteo, F. Lo Iacono, G. Navarra, A. Pirrotta, Direct evaluation of the equivalent linear damping for tld systems in random vibration for pre-design purposes, *International Journal of Non-Linear Mechanics* 63 (2014) 19–30. doi:10.1016/j.ijnonlinmec.2014.03.009.
- [21] D. K. Pandey, M. K. Sharma, S. K. Mishra, A compliant tuned liquid damper for controlling seismic vibration of short period structures, *Mechanical Systems and Signal Processing* 132 (2019) 405–428. doi:10.1016/j.ymsp.2019.07.002.
- [22] S. Lee, J. Park, B. Moon, K. Min, S. Lee, J. Kim, Design of a bracing-friction damper system for seismic retrofitting, *Smart Structures and Systems* 4 (5) (2008) 685–696. doi:10.12989/sss.2008.4.5.685.
- [23] A. Pisal, Seismic response of multi-story structure with multiple tuned mass friction dampers, *Int J Adv Struct Eng* 7 (2015) 81–92. doi:10.1007/s40091-014-0079-9.
- [24] N. Vaiana, M. Spizzuoco, G. Serino, Wire rope isolators for seismically base-isolated lightweight structures: Experimental characterization and mathematical modeling, *Engineering Structures* 140 (2017) 498–514. doi:10.1016/j.engstruct.2017.02.057.
- [25] A. F. Vakakis, O. Gendelman, Energy pumping in nonlinear mechanical oscillators, II: resonance capture, *Journal of Applied Mechanics* 68 (1) (2001) 42 – 48. doi:https://doi.org/10.1115/1.1345525.
- [26] A. F. Vakakis, O. V. Gendelman, L. A. Bergman, D. Michael McFarland, G. Kerschen, Y. S. Lee, *Nonlinear targeted energy transfer in mechanical and structural systems*, Springer, New - York, 2008.
- [27] E. Gourdon, N. A. Alexander, C. A. Taylor, C. H. Lamarque, S. Pernot, Nonlinear energy pumping under transient forcing with strongly nonlinear coupling: Theoretical and experimental results, *Journal of Sound and Vibration* 300 (3 - 5) (2007) 522–551. doi:10.1016/j.jsv.2006.06.074.
- [28] H. Ding, L. Chen, Designs, analysis, and applications of nonlinear energy sinks, *Nonlinear Dyn* 100 (2020) 3061–3107. doi:10.1007/s11071-020-05724-1.
- [29] P. O. Mattei, R. Ponçot, M. Pachebat, R. Côte, Nonlinear targeted energy transfer of two coupled cantilever beams coupled to a bistable light attachment, *Journal of Sound and Vibration* 373 (2016) 29–51. doi:10.1016/j.jsv.2016.03.008.
- [30] S. Lo Feudo, C. Touzé, J. Boisson, G. Cumunel, Nonlinear magnetic vibration absorber for passive control of a multi–storey structure, *Journal of Sound and Vibration* 438 (2019) 33–53. doi:10.1016/j.jsv.2018.09.007.
- [31] D. Michael McFarland, L. A. Bergman, A. F. Vakakis, Experimental study of non-linear energy pumping occurring at a single fast frequency, *Int. Journal of Non-linear Mechanics* 40 (2005) 891–899. doi:10.1016/j.ijnonlinmec.2004.11.001.
- [32] P. Zhou, H. Li, Modeling and control performance of a negative stiffness damper for suppressing stay cable vibrations, *Structural Control and Health Monitoring* 23 (4) (2016) 764 – 782. doi:https://doi.org/10.1002/stc.1809.
- [33] Y. Chen, Z. Qian, K. Chen, P. Tan, S. Tesfamariam, Seismic performance of a nonlinear energy sink with negative stiffness and sliding friction, *Structural Control and Health Monitoring* 26 (2019) e2437. doi:10.1002/stc.2437.
- [34] S. Benacchio, A. Malher, J. Boisson, C. Touzé, Design of a magnetic vibration absorber with tunable stiffnesses, *Nonlinear Dynamics* 85 (2016) 893–911. doi:10.1007/s11071-016-2731-3.
- [35] G. Pennisi, B. P. Mann, N. Naclerio, C. Stephan, G. Michon, Design and experimental study of a nonlinear energy sink coupled to an electromagnetic energy harvester, *Journal of Sound and Vibration* 437 (2018) 340–357. doi:10.1016/j.jsv.2018.08.026.
- [36] F. Romeo, L. I. Manevitch, L. A. Bergman, A. Vakakis, Transient and chaotic low-energy transfers in a system with bistable nonlinearity, *Chaos: An Interdisciplinary Journal of Nonlinear Science* 25 (5) (2015) 053109. doi:10.1063/1.4921193.
- [37] G. Pennisi, C. Stephan, E. Gourc, G. Michon, Experimental investigation and analytical description of a vibro-impact NES coupled to a single-degree-of-freedom linear oscillator harmonically forced, *Nonlinear Dynamics* 88 (3) (2017) 1769–1784. doi:10.1007/s11071-017-3344-1.
- [38] T. Li, S. Seguy, A. Berlioz, On the dynamics around target energy transfer for vibro-impact nonlinear energy sink, *Nonlinear Dynamics* 87 (2017) 1453 – 1466. doi:10.1007/s11071-016-3127-0.
- [39] T. Li, C. Lamarque, S. Seguy, A. Berlioz, Chaotic characteristic of a linear oscillator coupled with vibro-impact nonlinear energy sink, *Nonlinear Dynamics* 91 (4) (2018) 2319 – 2330. doi:https://doi.org/10.1007/s11071-017-4015-y.
- [40] F. Nucera, A. Vakakis, D. Michael McFarland, L. Bergman, G. Kerschen, Targeted energy transfers in vibro-impact oscillators for seismic

- mitigation, *Nonlinear Dyn* 50 (2007) 651–677. doi:10.1007/s11071-006-9189-7.
- [41] F. Nucera, F. Lo Iacono, D. Michael McFarland, L. Bergman, A. Vakakis, Application of broadband nonlinear targeted energy transfers for seismic mitigation of a shear frame: Experimental results, *Journal of Sound and Vibration* 313 (1) (2008) 57–76. doi:10.1016/j.jsv.2007.11.018.
- [42] F. Nucera, D. Michael McFarland, L. Bergman, A. Vakakis, Application of broadband nonlinear targeted energy transfers for seismic mitigation of a shear frame: Computational results, *Journal of Sound and Vibration* 329 (15) (2010) 2973–2994. doi:10.1016/j.jsv.2010.01.020.
- [43] J. Luo, N. E. Wierschem, S. A. Hubbard, L. A. Fahnestock, D. Dane Quinn, D. Michael McFarland, B. F. Spencer, A. F. Vakakis, L. Bergman, Large-scale experimental evaluation and numerical simulation of a system of nonlinear energy sinks for seismic mitigation, *Engineering Structures* 77 (2014) 34–48. doi:10.1016/j.engstruct.2014.07.020.
- [44] M. AL-Shudeifat, A. Saeed, Comparison of a modified vibro-impact nonlinear energy sink with other kinds of ness, *Meccanica* 3 (2020). doi:10.1007/s11012-020-01193-3.
- [45] Y. S. Lee, F. Nucera, A. F. Vakakis, D. Michael McFarland, L. A. Bergman, Periodic orbits, damped transitions and targeted energy transfers in oscillators with vibro-impact attachments, *Physica D: Nonlinear Phenomena* 238 (18) (2009) 1868–1896. doi:10.1016/j.physd.2009.06.013.
- [46] O. Gendelman, A. Alloni, Dynamics of forced system with vibro-impact energy sink, *Journal of Sound and Vibration* 358 (2015) 301 – 314. doi:https://doi.org/10.1016/j.jsv.2015.08.020.
- [47] F. Pacheco-Vasquez, S. Dorbolo, Rebound of a confined granular material: combination of a bouncing ball and a granular damper, in: *Scientific Reports*, Vol. 3, Nature, 2013, p. 2158.
- [48] M. Masmoudi, S. Job, M. Abbas, I. Tawfiq, M. Haddar, Experimental and numerical investigations of dissipation mechanisms in particle dampers, *Granular Matter* 18 (2016) 71. doi:10.1007/s10035-016-0667-4.
- [49] Z. Lu, Z. Wang, S. Masri, X. Lu, Particle impact dampers: Past, present, and future, *Structural Control and Health Monitoring* 25 (2018) e2058. doi:https://doi.org/10.1002/stc.2058.
- [50] Z. Lu, F. Masri, X. Lu, *Particle Damping Technology Based Structural Control*, Springer Tracts in Civil Engineering, Springer Singapore, 2020.
- [51] H. Li, C. Touzé, A. Pelat, F. Gautier, X. Kong, A vibro-impact acoustic black hole for passive damping of flexural beam vibrations, *Journal of Sound and Vibration* 450 (2019) 28–46. doi:10.1016/j.jsv.2019.03.004.
- [52] H. Li, C. Touzé, A. Pelat, F. Gautier, Combining nonlinear vibration absorbers and the acoustic black hole for passive broadband flexural vibration mitigation, *International Journal of Non-Linear Mechanics* (2020) 103558doi:10.1016/j.ijnonlinmec.2020.103558.
- [53] K. L. Johnson, *Contact Mechanics*, Cambridge University Press, 1985.
- [54] G. Kuwabara, K. Kono, Restitution coefficient in a collision between two spheres, *Japanese Journal of Applied Physics* 26 (8) (1987) 1230–1233. doi:10.1143/jjap.26.1230.
- [55] Y. Tsuji, T. Tanaka, T. Ishida, Lagrangian numerical simulation of plug flow of cohesionless particles in a horizontal pipe, *Powder Technology* 71 (3) (1992) 239–250. doi:10.1016/0032-5910(92)88030-1.
- [56] D. Antypov, J. A. Elliott, On an analytical solution for the damped hertzian spring, *EPL (Europhysics Letters)* 94 (5) (2011) 50004. doi:10.1209/0295-5075/94/50004.
- [57] E. Gourc, G. Michon, S. Séguy, A. Berlioz, Targeted energy transfer under harmonic forcing with a vibro-impact nonlinear energy sink: Analytical and experimental developments, *Journal of Vibration and Acoustics* 137 (3) (2015) 031008. doi:10.1115/1.4029285.
- [58] T. Li, E. Gourc, S. Seguy, A. Berlioz, Dynamics of two vibro-impact nonlinear energy sinks in parallel under periodic and transient excitations, *International Journal of Non-Linear Mechanics* 90 (2017) 100–110. doi:10.1016/j.ijnonlinmec.2017.01.010.
- [59] D. Qiu, S. Seguy, M. Paredes, Design criteria for optimally tuned vibro-impact nonlinear energy sink, *Journal of Sound and Vibration* 442 (2019) 497–513. doi:10.1016/j.jsv.2018.11.021.
- [60] K. Li, A. Darby, Modelling a buffered impact damper system using a spring-damper model of impact, *Structural Control and Health Monitoring* 16 (3) (2009) 287–302. doi:10.1002/stc.238.
- [61] A. Stevens, C. Hrenya, Comparison of soft-sphere models to measurements of collision properties during normal impacts, *Powder Technology* 154 (2005) 99–109. doi:10.1016/j.powtec.2005.04.033.
- [62] P. Flores, H. Lankarani, *Contact Force Models for Multibody Dynamics*, Vol. 226 of *Solid Mechanics and its Applications*, Springer, 2016.
- [63] I. Cook, Newton’s ‘experimental’ law of impacts, *The Mathematical Gazette* 70 (452) (1986) 107. doi:10.2307/3615768.
- [64] E. Falcon, C. Laroche, S. Fauve, C. Coste, Behavior of one inelastic ball bouncing repeatedly off the ground, *The European Physical Journal B* 3 (1998) 45–57. doi:10.1007/s100510050283.
- [65] M. Nagurka, S. Huang, Mass–spring–damper model of a bouncing ball, *International Journal of Engineering Education* 22 (2) (2006) 393 – 401.
- [66] S. Job, F. Melo, A. Sokolow, S. Sen, How hertzian solitary waves interact with boundaries in a 1d granular medium, *Phys. Rev. Lett.* 94 (2005) 178002. doi:10.1103/physrevlett.94.178002.
- [67] A. K. Chopra, *Dynamics of Structures*, 5th Edition, 5th Edition, Pearson, 2017.
- [68] T. Asami, O. Nishihara, A. Baz, Analytical solutions to H_{∞} and H_2 optimization of dynamic vibration absorbers attached to damped linear systems, *J. Vib. Acoust* 124 (2) (2002) 284–295. doi:10.1115/1.1456458.
- [69] M. Zilletti, S. Elliott, E. Rustighi, Optimisation of dynamic vibration absorbers to minimise kinetic energy and maximise internal power dissipation, *Journal of Sound and Vibration* 331 (18) (2012) 4093–4100. doi:10.1016/j.jsv.2012.04.023.
- [70] Y. Fujino, M. Abe, Design formulas for tuned mass dampers based on a perturbation technique, *Earthquake Eng Struct Dyn* 22 (10) (1993) 833–854. doi:10.1002/eqe.4290221002.
- [71] S. Krenk, Frequency analysis of the tuned mass damper, *Journal of Applied Mechanics* 72 (6) (2005) 936–942. doi:10.1115/1.2062867.
- [72] J. Connor, S. Laflamme, *Structural Motion Engineering*, Springer, Cham, 2014.
- [73] S. Etedali, H. Rakhshani, Optimum design of tuned mass dampers using multi-objective cuckoo search for buildings under seismic excitations, *Alexandria Engineering Journal* 57 (4) (2018) 3205–3218. doi:10.1016/j.aej.2018.01.009.

- [74] M. Chey, J. Chase, J. Mander, A. Carr, Semi-active tuned mass damper building systems: Design, *Earthquake Engineering and Structural Dynamics* 39 (2010) 119–139. doi:<https://doi.org/10.1002/eqe.934>.
- [75] D. Pietrosanti, M. D. Angelis, M. Basili, Optimal design and performance evaluation of systems with tuned mass damper inerter (tmdi), *Earthquake Engineering and Structural Dynamics* 46 (8) (2017) 1367–1388. doi:[10.1002/eqe.2861](https://doi.org/10.1002/eqe.2861).
- [76] S. Elias, Seismic energy assessment of buildings with tuned vibration absorbers, *Shock and Vibration* 2018 (2018) 1–10. doi:[10.1155/2018/2051687](https://doi.org/10.1155/2018/2051687).
- [77] M. Morales-Beltran, G. Turan, O. Dursun, R. Nijse, Energy dissipation and performance assessment of double damped outriggers in tall buildings under strong earthquakes, *Structural Design of Tall and Special Buildings* 28 (1) (2019) e1554. doi:<https://doi.org/10.1002/tal.1554>.